Analysis of Electron Spectra of Carbon Allotropes (Diamond, Graphite, Fullerene) by Density Functional Theory Calculations Using the Model Molecules

K. Endo,*,† S. Koizumi,† T. Otsuka,† T. Ida,† T. Morohashi,‡ J. Onoe,§ A. Nakao,§ E. Z. Kurmaev,|| A. Moewes,⊥ and D. P. Chong#

Department of Chemistry, Faculty of Science, Kanazawa University, Kanazawa 920-1192 Japan, Analytical Laboratory, Ulvac-PHI, Chigasaki 253-0084 Japan, The Institute of Physical and Chemical Research, Wako, Saitama 351-01 Japan, Institute of Metal Physics, Russian Academy of Sciences-Ural Division 620219, Yekaterinburg GSP-170 Russia, Department of Physics and Engineering Physics, University of Saskatchewan, 116 Science Place, Saskatoon, SK, Canada S7N 5E2, and Department of Chemistry, 2036 Main Mall, University of British Columbia, Vancouver, BC, Canada V6T 1Z1

Received: March 5, 2003; In Final Form: June 23, 2003

X-ray photoelectron, emission, and Auger electron spectra of diamond, graphite, and fullerene have been analyzed by deMon density-functional theory (DFT) calculations using the model molecules adamantane derivative ($C_{10}H_{12}(CH_3)_4$), pyrene ($C_{16}H_{10}$), and C_{60}, respectively. The theoretical valence photoelectron, C Kα X-ray emission, and Auger electron spectra for the allotropes are in good accordance with the experimental ones. The combination analysis of the valence X-ray photoelectron and C Kα X emission spectra enables us to divide the valence electronic distribution in the individual contributions for pσ- and pπ-bonding MOs of the carbon allotropes, respectively. The experimental Auger electron spectra of the allotropes can be classified in each range of 1s−2p2p, 1s−2s2p, and 1s−2s2s transitions for C KVV spectra, and in individual contributions of the chemically different carbon atoms from the theoretical analysis.

Introduction

Carbon allotropic forms of diamond, graphite and fullerene differ in their physical and chemical properties because of differences in the arrangement and bonding of tetrahedral sp^3, planer sp^2, and caged sp^2 carbons, respectively. Diamond films are desired for many applications,[1] including wear-resistant coatings, thin film semiconductor devices, X-ray lithographic membranes, and durable infrared windows. These films are usually deposited from gas-phase mixtures containing predominantly hydrogen.[2] For the graphite, it is well-known that the material is produced especially as very strong fibers by pyrolysis, at 1500 °C or above, of oriented organic polymer fibers. When incorporated into plastics, the reinforced materials are light and very strong. In the case of fullerene C_{60}, the material is expected to be applied in lubrication, coating, nonlinear optical and electronic devices, since the synthesis of the macroscopic quantities[3] and the surface modification[4] have been performed. It is, then, a very fundamental step to the design of the materials to examine the electronic state of the compounds from theoretical and experimental viewpoints.

Although differences in the structures between the allotropes will be reflected in the spectra by several analytical methods (X-ray photoelectron and emission spectroscopy, Auger electron spectroscopy, NMR, IR, and so on), there have been few studies that have dealt with such differences. In recent works,[5,6] we analyzed the valence X-ray photoelectron and emission spectra (XPS and XES) of diamond and graphite by the deMon density-functional theory (DFT) program[7] using the model molecules. In the work, we showed that the combined analysis of the XPS and C Kα XES enables us to divide the observed valence electronic distribution into the individual contributions for pσ- and pπ-bonding MOs of the allotropes. Thus, our aim in the present work is to perform the ultimate determination for analysis of the photoelectron, emission, and Auger electron spectra of the allotropes by the density functional theory (DFT) calculations. Here we demonstrate the combination analysis of the valence XPS, C Kα XES, and AES for the allotropes (diamond, graphite and fullerene) by deMon DFT calculations using the model adamantane derivative ($C_{10}H_{12}(CH_3)_4$), pyrene ($C_{16}H_{10}$), and C_{60} molecules, respectively.

Theoretical Background

(A) Energy. The generalized transition-state (GTS) method was proposed by Williams and co-workers[8] as an extension of Slater's transition-state method.[9] In the unrestricted GTS model, the endothermicity is approximated as

$$\Delta E = E(1) - E(0) = E_1 + E_2 + E_3 + E_4 + ... \quad (1)$$

by

$$\Delta E \approx \frac{F(0) + 3F(2/3)}{4} = E_1 + E_2 + E_3 + \frac{8}{9}E_4 + ... \quad (2)$$

where $F(\lambda) = \partial E(\lambda)/\partial\lambda$, $E(\lambda) = \Sigma\lambda^l E_l$, and λ ($0 \le \lambda \le 1$) is assumed to be a continuous variable. $E(0)$ and $E(1)$ denote the energies of the initial and final states, respectively. For the ionization of an electron from molecular orbital (MO) ϕ_l of interest, λ represents the fraction number of electron removed from the Kohn−Sham (KS) MO. According to the Janak

† Kanazawa University.
‡ Ulvac-PHI.
§ Institute of Physical and Chemical Research.
|| Russian Academy of Sciences.
⊥ University of Saskatchewan.
University of British Columbia.

10.1021/jp0345710 CCC: $25.00
Published on Web 10/10/2003

theorem,[10] $F(\lambda)$ becomes the negative KS orbital energy, $\epsilon_l(\lambda)$. For the calculation of core−electron binding energies (CEBE-(I_c)), this procedure is applied in the following way. In the unrestricted generalized transition-state (uGTS) method, we removed the 2/3 electron from the inner core−electron level KS MO ϕ_l.

For the vertical ionization potentials (VIP(I_k)) of the valence regions, we used the restricted generalized diffuse ionization (rGDI) model,[11] which is just the extension of the restricted diffuse ionization (rDI) model that Åsbrink and co-workers proposed in the HAM/3 method.[12] In the rGDI model, as indicated in the work,[11] the 2/3 electron is removed evenly from all α and β valence MOs and the negative resulting orbital energies are approximated as $F(2/3)$ for each valence MO. Thus, we obtain each valence VIP using eq 2.

In the case of C Kα X-ray emission energy, we obtain the value from the difference ($I_c - I_k$) between the carbon 1s CEBE of the hole and VIP of electrons to fill up the hole.

The calculation of Auger electron energy may be expressed in terms of the single hole binding energy for an electron in the core orbital, I_c at the initial state, and the double hole ionization energy in the valence orbital, $I_{VV'}$ at the final state. The $I_{VV'}$ is often expressed as the sum of two single ionization energies (I_j, I_k^*). We can then give the Auger electron energy in the following way,

$$E_{cjk} = I_c - I_j - I_k^* \tag{3}$$

where I_c and (I_j, I_k^*) denote the CEBE and VIPs. The VIP, I_k^* is the ionization energy of an electron from the *k*th MO of the singly ionized cation (which has already lost an electron from the *j*th MO).

To explain the solid-state effect, we define a quantity *WD* as stated in early works.[13−17] This quantity *WD* denotes the sum of the work function of the sample (*W*) and other energy effects (*D* as delta), such as the polarization energy, the width of the intermolecular band formation, and the peak broadening in the solid state. The experimental *WD* can be estimated from difference between theoretical electron binding energy (I_c, or I_k) of model molecules, and the experimental binding energy of the allotropes. Therefore, for the comparison between the calculated energy (I_c or I_k) for single molecules of cluster model and experimental binding energy (I'_c or I'_k) of solid allotropes, we must shift each computed (I_c, or I_k) by a quantity *WD* as I'_c ($=I_c - WD$) {or I'_k ($=I_k - WD$)}, to convert to I'_c (or I'_k) relative to the Fermi level.

(B) Intensity. The intensity of valence XPS was estimated from the relative photoionization cross-section for Al Kα radiation using the Gelius intensity model.[18] For the relative atomic photoionization cross-section, we used the theoretical values from Yeh.[19]

The XES intensity of carbon spectral lines was obtained by summing the LCAO populations $P_{j[2p(A)]l}$ of the atomic orbitals $\chi_{2p(A)}(r)$ centered on given carbon atoms; $l = x$, y, and z. In the case of C Kα spectra, the XES transition arises from outer occupied p orbitals to s-type holes in a given atom, due to the selection rule $\Delta l = \pm 1$.

Considering the selection rule and neglecting the terms involving orbital products on different atoms, an approximate intensity $RI_{1s(A)j}$ is given by

$$RI_{1s(A)j} = N' \sum_{A} |C_{j[2p(A)]l}|^2 \tag{4}$$

where N' is a constant for each particular spectrum, and $C_{j[2p(A)]}$ is the LCAO coefficient of the atomic orbital $\chi_{2p(A)}(r)$ centered on atom A.

The relative Auger transition probability from an initial core hole to the final state with two hole in valence region and an electron in the continuum was expressed by Wentzel,[20]

$$M_{CVV'} = \sum_{\epsilon} \left| \left\langle \Psi(c,\epsilon) \left| \sum_{i,j} \frac{1}{r_{ij}} \right| \Psi(v,v') \right\rangle \right|^2 \tag{5}$$

Here $\Psi(c\epsilon)$ is the total wave function, which denotes the core hole, c, and final-state continuum, ϵ, orbitals, respectively; the other total wave function $\Psi(v,v')$ involves the two final-state hole orbitals in valence levels.

Ramarker and co-workers[21,22] proposed the one-center intensity model for the calculation of Auger electron intensities of solid SiO_2. The relative Auger intensities are given as

$$M_{cjk} = N' \sum_{\mu,\nu} |C_{\mu j}|^2 |C_{\nu k}|^2 P_{c\mu\nu} \tag{6}$$

Here $|C_{\mu j}|^2$ and $|C_{\nu k}|^2$ represent the electron density populations of the atomic orbitals, ψ_μ and ψ_ν, respectively, on the central atom A associated with the molecular orbitals, ϕ_j and ϕ_k. N' and $P_{c\mu\nu}$ denote a statistical factor and the appropriate weighted subshell Auger transition probabilities, respectively. In our calculation of the relative Auger intensities, we used eq 6 and adopted the theoretical values of the subshell Auger transition probabilities from Chen and co-workers.[23]

Calculation Details

The calculations have been performed within the cluster model approach. The cluster dangling bonds of diamond and graphite except for fullerene have been saturated with H atoms. The model molecules [adamantane derivative ($C_{10}H_{12}(CH_3)_4$), pyrene ($C_{16}H_{10}$), and fullerene C_{60}] were calculated by the deMon-KS DFT program.[7] For the geometry of the molecules, we used the optimized Cartesian coordinates from the semi-empirical AM1 (version 6.0) method.[24]

The deMon calculations were performed with the exchange-correlation potential labeled as B88/P86, made from Becke's 1988 exchange functional,[25] and Perdew's 1986 correlation functional.[26] In the program, we used a nonrandom grid and a polarized valence double-ζ (DZVP) basis of (621/41/1*) for C, and (41) for H with auxiliary fitting functions labeled (4, 4; 4, 4) for C, and (3, 1; 3, 1) for H. To calculate each intensity of XES at each emission energy for model molecules, we used the STO-3G basis set for all atoms of the model molecules.

To simulate the valence XPS and XES of carbon allotropes theoretically, we constructed from a superposition of peaks centered on each VIP, I_k and each emission energy, ($I_c - I_k$), respectively. As was done in previous works,[5,6,13−15] each peak was represented by a Gaussian curve. In the case of the line width ($WH(k)$), we used $WH(k) = 0.10\ I_k$ (proportional to the ionization energy) for valence XPS, and $WH(k) = 1.5$ eV (experimental resolution) for C Kα XES, respectively.

In the calculations of the CEBEs, we used a polarized valence double-ζ (DZVP)) basis set for the model molecules in the initial state and the scaled polarized valence double-ζ (DZVP) basis set in the uGTS model.

To simulate the AES of the carbon allotropes, we constructed, from a superposition of peaks centered on the Auger electron energies, ($I_c - I_j - I_k^*$) in the each central atom *A* on the

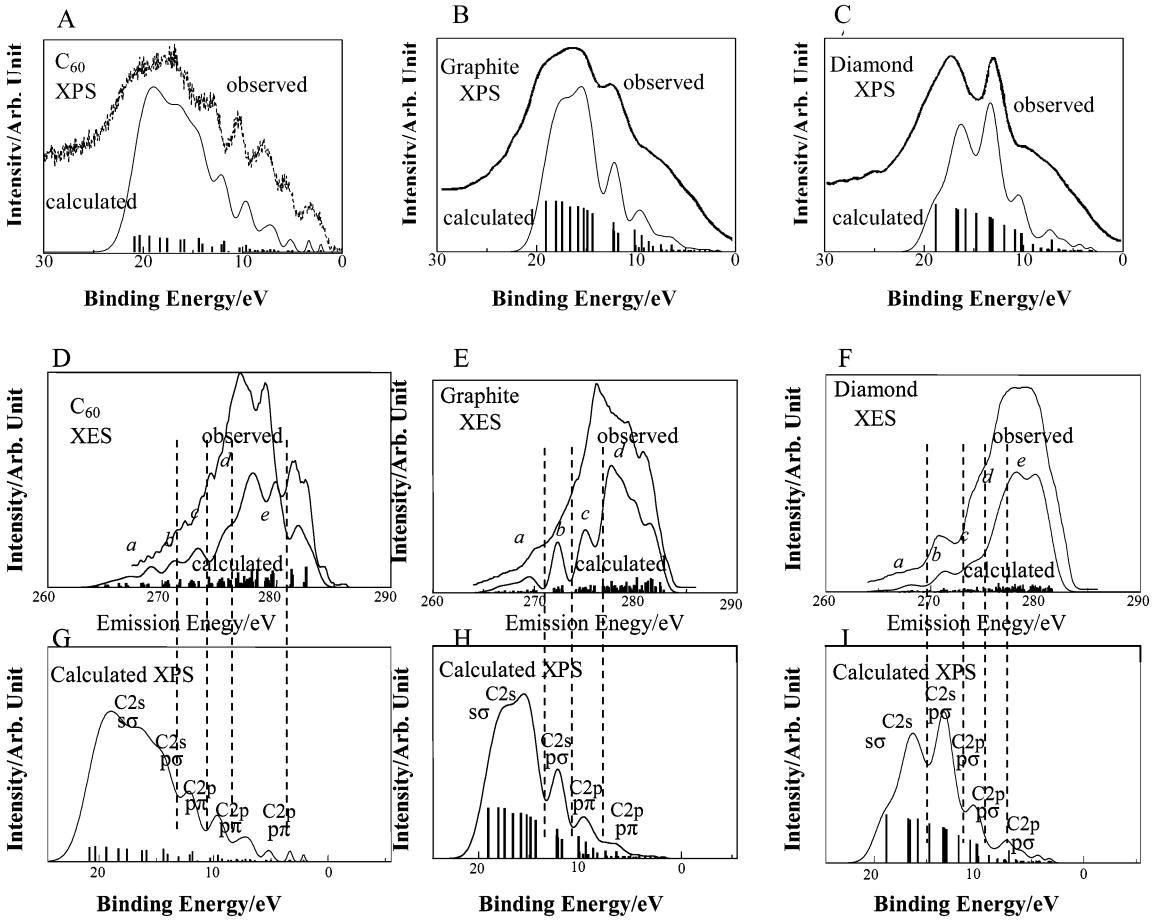

Figure 1. (A) experimental and calculated valence XPS of fullerene. (B) Experimental and calculated valence XPS of graphite. (C) Experimental and calculated valence XPS of diamond. (D) Experimental and calculated XES of fullerene. (E) Experimental and calculated XES of graphite. (F) Experimental and calculated XES of diamond. (G) Calculated valence XPS of fullerene. (H) Calculated valence XPS of graphite. (I) Calculated valence XPS of diamond.

TABLE 1: Observed Peak, VIP, Main AO Photoionization Cross-Section, Orbital Nature, and Functional Group for X-ray Photoelectron Spectra of Carbon Allotropes

observed peak (eV)	VIP (eV)	main AO photoionization cross-section	orbital nature	functional group
		Fullerene		
18.0 (15.0−24.0)[a]	23.08−26.36	C2s	sσ(C2s−C2s)-B	−C═C
14.0 (12.0−15.0)[a]	19.53−21.75	C2s	s,pσ(C2s−C2s,p)-B	−C═C
11.0 (10.0−12.0)[a]	17.35−18.56	C2s,C2p	pσ,π(C2s,p−C2p)-B	−C═C
8.0 (6.0−10.0)[a]	13.38−15.80	C2p	pπ(C2p−C2p)-B	−C═C
5.0 (4.0−6.0)[a]	9.76−13.00	C2p	pπ(C2p−C2p)-B	−C═C
3.0 (1.0−4.0)[a]	7.63−9.50	C2p	pπ(C2p−C2p)-B	−C═C
		Graphite		
16.0 (13.0−23.0)[a]	19.88−24.67	C2s	sσ(C2s−C2s)-B	−C═C
12.5 (10.5−13.0)[a]	17.35−17.83	C2s	s,pσ(C2s−C2s,p)-B	−C═C
10.0 {shoulder	13.76−15.64	C2p	pπ(C2p−C2p)-B	−C═C
peak (2.0−10.5)[a]}	7.30−12.53	C2p	pπ(C2p−C2p)-B	−C═C
		Diamond		
19.0 (16.0−23.0)[a]	20.24−24.32	C2s	sσ(C2s−C2s)-B	−C(f)−C(f)
15.0 (13.0−16.0)[a]	18.59−18.91	C2s	sσ(C2s−C2s)-B	−C(f)−C(f), −C(f)−C(p)
10.0 {shoulder	15.66−16.34	C2s	pσ(C2s−C2p)-B	−C(f)−C(f), −C(f)−C(p)
peak (2.0−12.0)[a]}	13.01−13.78	C2p	pσ(C2p−C2p)-B	−C(f)−C(p)
	8.60−12.65	C2p	pσ(C2p−C2p)-B	−C(f)−C(f), −C(f)−C(p)

[a] Shows the peak range. WD(difference between calculated and observed peaks) = 5.5 eV.

assumption that Auger process dominated by the intra-atomic transition. Each peak was represented by Gaussian line shape functions of a fixed line width 3 eV (experimental resolution) for the AES.

Experimental Section

We used a diamond film as deposited from a gas-phase mixture containing hydrogen, graphite as produced by pyrolysis, and commercially available fullerene C_{60} (Aldrich chemical Co.

TABLE 2: Observed Peak, Emission Energy, Orbital Nature and Functional Group for C Kα X-ray Emission Spectra of Carbon Allotropes

observed peak (eV)	emission energy (eV)	orbital nature	functional group
	Fullerene		
265−271[a]	263.4−270.4 {a in Figure 1F}	sσ(C2s−C2s)-B	−C═C
271−274[a]	270.9−272.8 {b in Figure 1F}	pσ(C2s−C2p)-B	−C═C
274−276[a]	273.2−276.0 {c in Figure 1F}	pπ(C2p−C2p)-B	−C═C
276−281[a]	276.5−279.7 {d in Figure 1F}	pπ(C2p−C2p)-B	−C═C
281−283[a]	280.9−282.6 {e in Figure 1F}	pπ(C2p−C2p)-B	−C═C
	Graphite		
265−271[a]	265.0−271.0 {a in Figure 1E}	sσ(C2s−C2s)-B	−C═C
271−273[a]	271.9−272.8 {b in Figure 1E}	pσ(C2s−C2p)-B	−C═C
273−276[a]	274.1−276.0 {c in Figure 1E}	pπ(C2p−C2p)-B	−C═C
276−283[a]	276.2−282.8 {d in Figure 1E}	pπ(C2p−C2p)-B	−C═C
	Diamond		
265−269[a]	265.0−269.7 {a in Figure 1D}	sσ(C2s−C2s)-B	−C(f)−C(f)
269−272[a]	270.9−272.5 {b in Figure 1D}	pσ(C2s−C2p)-B	−C(f)−C(f), −C(f)−C(p)
272−275[a]	273.0−275.0 {c in Figure 1D}	pσ(C2p−C2p)-B	−C(f)−C(f), −C(f)−C(p)
275−277[a]	275.4−276.9 {d in Figure 1D}	pσ(C2p−C2p)-B	−C(f)−C(f)
277−283[a]	277.1−281.6 {e in Figure 1D}	pσ(C2p−C2p)-B	−C(f)−C(f), −C(f)−C(p)

[a] Shows the peak range.

Inc), respectively. For the diamond film, it was grown by flowing a mixture of 99.5% H_2 and 0.5 % CH_4 at a pressure of 50 Torr through a tungsten filament heated to 2000 °C onto a silicon wafer substrate heated to 850 °C. The thickness of the film was kept as about 2 μm at the growth rate of 0.5 μm/h.

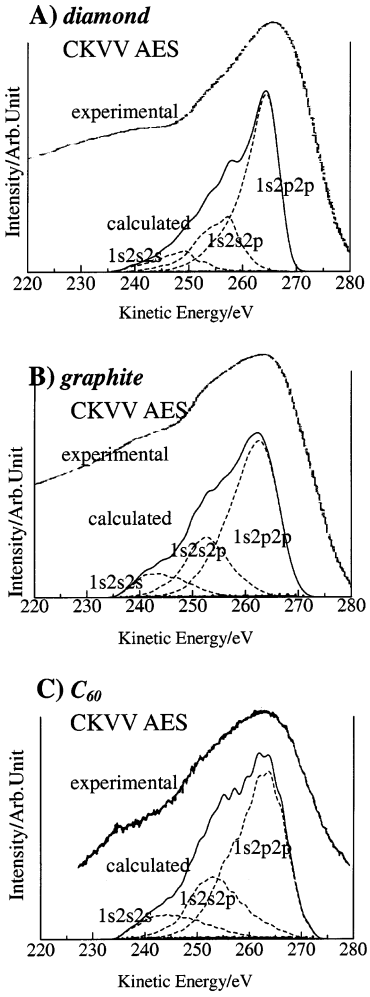

Figure 2. (A) experimental and calculated carbon KVV′ AES of diamond. (B) Experimental and calculated carbon KVV′ AES of graphite. (C) Experimental and calculated carbon KVV′ AES of fullerene.

The experimental photoelectron and Auger electron spectra of the samples were obtained on a PHI 5400 MC ESCA spectrometer, using monochromatized Al Kα radiation. We obtained the Auger electron spectrum of the fullerene using the monochromatized Al Kα radiation, to reduce the charging effect on the surface of the sample. The spectrometer was operated at an X-ray Al Kα source power at 600 W, at a constant voltage of 15 kV, and at a constant current of 40 mA. The photon energy was 1486.6 eV. A pass energy of 71.55 eV was employed for high-resolution scans in a valence-band analysis (50 eV of range). The angle between the X-ray source and the analyzer was fixed at spot 45°. The size in the measurement was 3 × 1 mm.[2]

The use of dispersion compensation yielded an instrumental resolution of 0.5 eV with the full width at half-maximum on the Ag3d line of silver. Multiple-scan averaging on a multichannel analyzer was used for the valence band region, although

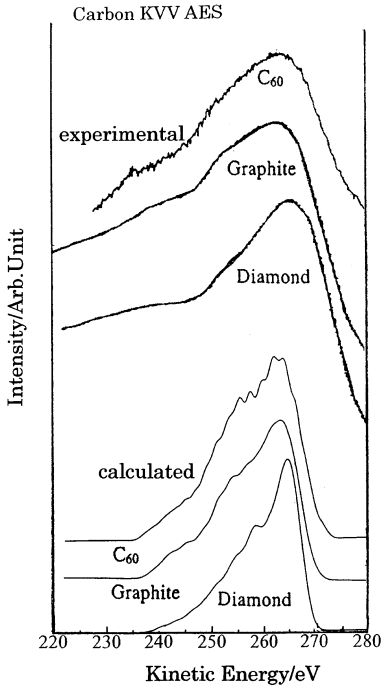

Figure 3. Observed and calculated carbon KVV′ AES of diamond, graphite, and fullerene, respectively.

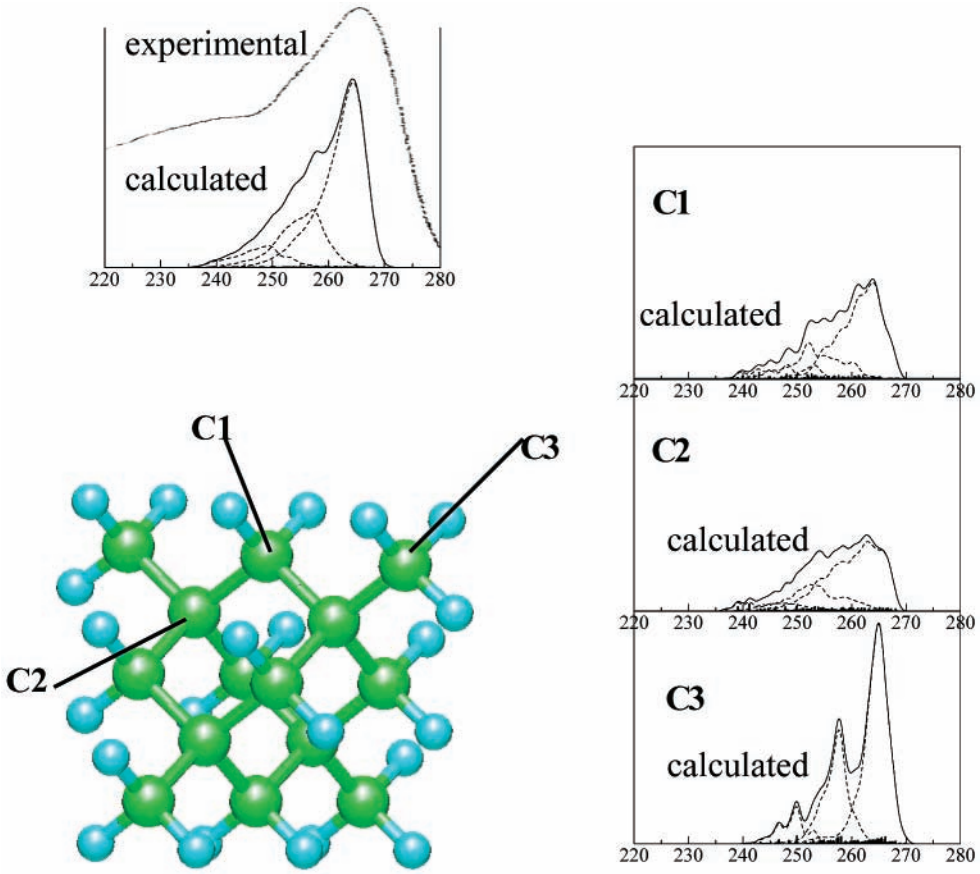

Figure 4. Ball-stick structure of the adamantane derivative ($C_{10}H_{12}(CH_3)_4$) in the unit cell for the diamond model molecule, experimental and calculated AES of diamond, and calculated AES in individual contributions from the chemically different carbon atoms.

a very low photoelectron emission cross-section was observed in this range.

Gold of 20 Å thickness was deposited on the film (or disk) of the samples using an ion sputter unit (Hitachi E 1030) for the scanning electron microscope.

A low-energy electron flood gun was used to avoid any charging effect on the surface of the sample. We used the Au 4f core level of the gold decoration membrane (or disk) as a calibration reference. The C1s line positions of diamond and graphite could be fixed at 285.0 eV, respectively.

Due to the inherently low yield of the soft X-ray emission process, we made use of the high brightness available at Lawrence Berkeley National Laboratory's Advanced Light Source (ALS). The spectra were taken Beamline 8.0, employing the University of Tennessee at Knoxville's soft X-ray fluorescence (SXF) endstation.[27] Photons with an energy of 320 eV, above the carbon K edge were delivered to the endstation via the beamline's 89-period, 5-centimeter indulator insertion device and spherical grating monochromator. The SXF endstation consists of an ultrahigh vacuum (pressure below 10^{-9} Torr) sample manipulation chamber connected to a Rowland circle grating spectrometer that is equipped with four interchangeable spherical diffraction gratings, and a position sensitive microchannel detector. The position sensitive detector is moved along the Rowland circle to the region of interest for the emission measurements. We obtained each emission measurement with just 10−20 min of exposure. All measurements reported here were made with the 100 μm entrance slit for the spectrometer. The carbon Kα spectra were obtained with a 600 lines/mm, 10 m radius grating. The carbon Kα emission spectra were calibrated with a reference sample of highly oriented pyrolytic graphite. At the carbon K edges the resolution of the spectrometer was approximately 0.3−0.4 eV.

Results and Discussion

Although the electronic states of diamond[28,29] and graphite,[30] respectively, were investigated from analysis of valence XPS and XES using band theory of the one-electron partial density of states (DOS), the workers[29,30] did not sufficiently explain the electronic orbital nature of each peak for the experimental spectra of diamond and graphite. As far as we know, there is no study on the electronic states of fullerene from analysis of XPS and XES using MO and DFT methods. In this section, we perform the detailed analysis for valence XPS, XES, and AES of the diamond, graphite, and fullerene by the DFT calculations using the model molecules.

The carbon form of diamond is almost invariably found with the cubic structure. It exists as a hexagonal form found in certain meteorites and available synthetically. The hexagonal form is probably unstable toward the cubic, because, unlike the cubic, it contains some eclipsed bonds. The hexagonal form in the unit cell is similar to the carbon frame of the adamantane derivative. We, thus, used the adamantane derivative ($C_{10}H_{12}$-$(CH_3)_4$) to simulate XPS, XES, and AES of a diamond-like film. In the case of graphite, it has a layer structure of benzene rings. The separation of the layers is 3.35 Å, which is about equal to the sum of van der Waals radii. It is noted that within each layer each carbon is surrounded with only three others. After forming one σ bond with each neighbor, each carbon would still have one electron and these are paired up into a system of π bonds. We adopted the pyrene as the model molecule of graphite, because it consists of four benzene rings. In the case of fullerene, we used the C_{60} molecule itself.

(a) XPS and XES of the Allotropes. To clarify the combination analysis of theoretical and experimental valence XPS and XES, we show in superimposition in Figure 1A−I for fullerene, graphite, and diamond, respectively. In Figure 1A−I, X-ray photoelectron and emission spectra reflect the differences of the chemical structures among fullerene, graphite, and diamond. In Table 1, we show the observed peak and calculated VIP, main contributions of atomic orbital photoionization cross-section, orbital nature, and the functional groups for valence X-ray photoelectron spectra of the allotropes.

For C Kα X-ray emission spectra, the calculated C Kα XES from the model molecules [fullerene (C_{60}), pyrene ($C_{16}H_{10}$) and adamantane derivative ($C_{10}H_{12}(CH_3)_4$)] are found to be in good agreement with experimental X-ray emission spectra of fullerene, graphite, and diamond, respectively (see Figure 1D−F). In Table 2, we showed observed peak, emission energy, orbital nature, and functional group for XES of the allotropes. In (D)−(F), we classified the orbital nature of each emission spectrum for the allotropes into four or five ranges between 265 and 285 eV, as shown in (a)−(e) or (a)−(d) partitioned with column lines (the classification was also shown in Table 2). The areas of (a)−(d) or (a)−(e) partitioned with lines in Figure 1D−F correspond to those of the calculated valence spectra in Figure 1G−I.

(b) AES of the Allotropes. Figure 2A−C shows Auger electron spectra of the carbon allotropes plotted as the intensity versus the kinetic energy of the Auger electron in each carbon atom, because the kinetic energy is approximately equal to the Auger electron energy, $[(\mathrm{CEBE}, I_c^A)_{1s} - (\mathrm{VIP}, I_j) - (\mathrm{VIP}', I_k^*)]$ in the each central atom *A*. In the figure, the simulated AES for the diamond-like film, graphite, and fullerene, respectively, are in good accordance with the experimental spectra. In simulated spectra, we showed total carbon KVV AES with solid lines and the individual 1s−2p2p, 1s−2s2p, and 1s−2s2s transition spectra with dashed lines, respectively.

In Figure 3, the experimental peaks of carbon KVV AES for fullerene and graphite seem to be broader than that of the diamond-like film, although the main peaks of the carbon allotrope result from the superimposition of 1s−2s2p and 1s−2p2p, respectively. The broader peaks of fullerene and graphite depend on pπ orbitals of aromatic carbons, whereas the sharp peak of the diamond-like film is due to pσ orbitals of aliphatic carbons. To clarify the origin of the sharp peak for the diamond-like film, we simulated the individual spectra due to the different kinds of carbon atoms. Figure 4 indicates a ball-stick structure of the adamantane derivative ($C_{10}H_{12}(CH_3)_4$) in the unit cell for the diamond-like film model and simulated AES in individual contributions from the different kinds of carbons (in the unit cell, we think C1 and C2 atoms exist in the adamantane frame and pendant methyl C3 carbons are on the lattices of the unit cell). In Figure 4, it is characteristic that the Auger electron spectrum due to 1s−2p2p, 1s−2s2p, and 1s−2s2s transitions of the C3 carbon groups is the sharpest in the three kinds of carbons. On the other hand, AES from other C1 and C2 carbons are broader. Thus, the sharpest peak of the diamond-like film in comparison with the peaks of the graphite and fullerene results mainly from the methyl carbons C3 on the lattices of the unit cell, because the total peak is due to the superimposition of the individual C1, C2, and C3 carbon atoms.

Conclusions

We demonstrate the combination analysis of the valence XPS, C Kα XES, and AES for the allotropes (diamond-like film, graphite, and fullerene) by deMon DFT calculations using the model adamantane derivative ($C_{10}H_{12}(CH_3)_4$), pyrene ($C_{16}H_{10}$), and C_{60} molecules, respectively.

The theoretical valence photoelectron, C Kα X-ray emission, and Auger electron spectra for the allotropes are in good accordance with the experimental ones. The combination analysis of the valence XPS and C Kα XES enables us to divide the valence electronic distribution in the individual contributions for pσ- and pπ-bonding MOs of the carbon allotropes, respectively. The experimental AES of the allotropes can be classified in each range of 1s−2p2p, 1s−2s2p, and 1s−2s2s transitions for C KVV spectra, and in individual contributions of the chemically different carbon atoms from the theoretical analysis. Especially, the sharpest peak of the diamond-like film in comparison with the peaks of the graphite and fullerene results mainly from the carbons on the lattices of the unit cell for the diamond, because the total peak is due to the superimposition of the individual carbon atoms in the unit cell.

As far as we know, the X-ray photoelectron, emission, and Auger electron spectra for the diamond-like film (2 μm-thickness) are similar to those of bulk diamond. Our analysis due to the adamantane derivative enables us not only to use that of AES for bulk diamond but also to do analyses of the XPS and the XES.

References and Notes

(1) Angus, J. C.; Hayman, C. C. *Science* **1988**, *241*, 919.
(2) DeVries, R. C. *Annu. Rev. Mater. Sci.* **1987**, *17*, 161.
(3) David, T.; Gimzewski, J. K.; Purdie, D.; Reihl, B.; Schlitter, R. R. *Phys. Rev.* **1994**, *B50*, 5810.
(4) Onoe, J.; Nakao, A.; Takeuchi, K. *Phys. Rev.* **1997**, *B 55*, 10051.
(5) Endo, K.; Morohashi, T.; Otsuka, T.; Koizumi, S.; Suhara, M.; Chong, D. P. *J. Surf. Anal.* **1999**, *6*, 186.
(6) Endo, K.; Koizumi, S.; Otsuka, T.; Suhara, Morohashi, T.; Kurmaev, E. Z.; Chong, D. P. *J. Comput. Chem.* **2001**, *22*, 102.
(7) St-Amant, A.; Salahub, D. R. *Chem. Phys. Lett.* **1990**, *169*, 387. St-Amant A. Ph.D. Thesis, University of Montreal, 1991.
(8) Williams, A. R.; deGroot, R. A.; Sommers, C. B. *J. Chem. Phys.* **1975**, *63*, 628.
(9) Slater, J. C. *Adv. Quantum Chem.* **1972**, *6*, 1.
(10) Janak, J. F. *Phys. Rev.* **1978**, *A 18*, 7165.
(11) Duffy, P.; Chong, D. P. *Org. Mass. Spectrom.* **1993**, *28*, 321.
(12) Asbrink, L.; Fridh, C.; Lindholm, E. *Chem. Phys. Lett.* **1977**, *52*, 69.
(13) Endo, K.; Kaneda, Y.; Aida, M.; Chong, D. P. *J. Phys. Chem. Solids* **1995**, *56*, 1131.
(14) Endo, K.; Inoue, C.; Kaneda, Y.; Aida, M.; Kobayashi, N.; Chong, D. P. *Bull. Chem. Soc. Jpn.* **1995**, *68*, 528.
(15) Endo, K.; Kaneda, Y.; Okada, H.; Chong, D. P.; Duffy, P. J. *Phys. Chem.* **1996**, *100*, 19455.
(16) Endo, K.; Chong, D. P. *J. Surf. Anal.* **1997**, *3*, 618; **1998**, *4*, 50.
(17) Kuroki, S.; Endo, K.; Maeda, S.; Chong, D. P.; Duffy, P. *Polym. J.* **1998**, *30*, 142.
(18) Gelius, U.; Siegbahn, K. *Faraday Discus. Chem. Soc.* **1972**, *54*, 257. Gelius U. *J. Electron. Spectrosc. Relat. Phenom.* **1974**, *5*, 985.
(19) Yeh, J.-J. *Atomic Calculation of Photoionization Cross Section and Asymmetry Parameters*; Gordon and Breach Science Publishers: New York, 1993.
(20) Wentzel, G. Z. *Phys.* **1927**, *43*, 524.
(21) Ramarker, D. E.; Murday, J. S.; Turner, N. H.; Moore, G.; Lagally, M. G.; Houston, J. *Phys. Rev.* **1979**, *B 19*, 5375.
(22) Ramarker, D. E. *Phys. Rev.* **1980**, *B 21*, 4608.
(23) Chen, M. H.; Larkins, F. P.; Crasemann, B. *At. Data Nucl. Data Tables* **1990**, *45*, 1.
(24) Dewar, M. J. S.; Dewar, E. G. *THEOCHEM* **1988**, *180*, 1. Dewar, M. J. S.; Dewar, E. G.; Healy, E. F.; Stewart, J. J. P. *J. Am. Chem. Soc.* **1985**, *107*, 3902.
(25) Becke, A. D. *Phys. Rev.* **1988**, *A 38*, 3098.
(26) Perdew, J. P. *Phys. Rev.* **1986**, *B 33*, 8822.
(27) Jia, J. J.; Callcott, T. A.; Yurkas, J.; Ellis, A. W.; Himpsel, F. J.; Samant, M. G.; Stöhr, J.; Ederer, D. L.; Perera, R. C. C. *Rev. Sci. Instrum.* **1995**, *66*, 1394.
(28) Cavell, R. G.; Kowalczyk, S. P.; Ley, L.; Pollak, R. A.; Mill, B.; Shirley, D. A.; Perry, W. *Phys. Rev.* **1973**, *B7*, 5313.
(29) Aleshin, V.G.; Kucherenko, Yu. N. *J. Electron Spectrosc. Relat. Phenom.* **1976**, *8*, 411.
(30) Murday, J. S.; Dunlap, B. I.; Hutson, F. L., II; Oelhafen, P. *Phys. Rev.* **1981**, *B24*, 4764.